Emergence of a quantum coherent state at the border of ferroelectricity

M.J. Coak[1*], C.R.S. Haines[1*], C. Liu[1], S.E. Rowley[1,2], G.G. Lonzarich[1] and S.S. Saxena[1,3*]

1. Cavendish Laboratory, Cambridge University, J.J. Thomson Ave, Cambridge CB3 0HE, UK

2. Centro Brasileiro de Pesquisas Fisicas, Rua Dr. Xavier Sigaud 150, Rio de Janeiro 22290-180, Brazil

3. National University of Science and Technology "MISiS", Leninsky Prospekt 4, Moscow 119049, Russia

* Corresponding author

Quantum melting of magnetism or ferroelectricity can lead to novel forms of order characterized by exotic excitations and unconventional superconductivity. Here we show by means of high precision measurements of the temperature and pressure dependence of the dielectric susceptibility that quantum melting of a displacive ferroelectric leads to an unconventional quantum paraelectric state exhibiting the phenomenon of "order by disorder", namely a fluctuation induced enhancement of electric polarization extending up to a characteristic coherence temperature T^*. T^* vanishes at the ferroelectric quantum critical point and the square of T^* increases with a characteristic linear dependence on the applied pressure. We show that in the vicinity of T^* this thermal activation phenomenon can be understood quantitatively, without the use of adjustable parameters, in terms of the hybridization of the critical electric polarization field and the volume strain field of the lattice. At still lower temperatures, well below T^*, we observe a breakdown of this unconventional form of quantum paraelectricity and the emergence of a still more exotic state characterized by slowly fluctuating micro-domains of the lattice structure. We suggest that this low temperature state may be viewed as a type of instanton liquid arising from anisotropic strain induced long-range correlations of the electric polarization field.

Introduction

The study of quantum phase transitions and quantum critical systems has led to the discovery of novel phases of matter and the introduction of novel conceptual frameworks for the description of emergent phenomena [1–9]. A quantum phase transition reached by varying a tuning parameter such as lattice density or electronic band filling fraction is imagined to separate two or more low-temperature states with qualitatively different types of order that may or may not be defined in terms of transparent local order parameters as conventionally defined. An example is a transition from a magnetically polarized to a paramagnetic state in a metal [10–14]. In the Kondo lattice model, for instance, the Fermi liquid state is a particularly exotic state characterized by the existence of composite quasiparticle excitations created by the collective hybridization of conduction electron and localized electron orbitals, a phenomenon that has reached a relatively advanced level of description.

Another example involves a transition from a displacive ferroelectric state to an unpolarized or quantum paraelectric state in polar materials such as the perovskite oxides [15–34]. In contrast to the case of the magnetic metals the nature of the unpolarized state in incipient ferroelectrics remains an enigma. In the simplest model the quantum paraelectric state is characterized by an activated form of the temperature dependence of the inverse dielectric susceptibility in which the activation temperature vanishes at a continuous quantum phase transition, i.e., at a quantum critical point. However, this picture has proved to be insufficient and in particular is contradicted by the observation of an anomalous temperature dependence - including a mysterious minimum - in the inverse susceptibility of $SrTiO_3$ and related incipient displacive ferroelectrics at low temperat-

1

ures [28, 29, 32, 35], which recent theoretical works have attempted to describe [16, 25, 28].

The identification of the nature of the hidden order characterizing the quantum paraelectric states in such materials has been a key objective of the present study. This is a part of a more general goal to characterize and understand the temperature-quantum tuning parameter phase diagram of quantum critical ferroelectrics.

The absence of free charge carriers (in the undoped samples) was expected to lead to a simpler phase diagram than that observed near to quantum critical points in metals, in which quantum critical phenomena are in many interesting cases masked by the emergence of intervening phases. These include unconventional superconductivity and exotic textured phases, which are of great interest but stand in the way of understanding quantum critical behaviours in their simplest forms over wide ranges down to very low temperatures.

To characterize the temperature-quantum tuning parameter phase diagram in close detail and identify the nature of the mysterious hidden order state we have carried out measurements of the dielectric response over a wide range in temperature and pressure with extreme precision. In particular, the identification of the low temperature behaviour of the relative dielectric constant, ε_r, or dielectric susceptibility, $\chi = \varepsilon_r - 1$, has benefited from measurements of relative changes of χ as small as a few parts per billion. We first mention briefly the results of some relevant previous studies of our chosen material and then present and discuss our new findings.

$SrTiO_3$ is a well-studied incipient displacive ferroelectric [36], widely used as a dielectric in deposition techniques and thin-film interface devices [37], as well as recently in high-precision thermometry [38], and is remarkable for having an extremely high dielectric susceptibility at low temperatures. At high temperatures a good fit to the classically predicted Curie-Weiss form of the dielectric susceptibility is observed, with an extrapolated Curie Temperature around 35 K [39], but this temperature dependence changes below approximately 50 K in the quantum critical regime and no ferroelectric ordering occurs down to the lowest temperatures measured. In addition, substitution of oxygen-16 for the oxygen-18 isotope results in the material becoming ferroelectric, and varying the level of isotope substitution or applying pressure tunes the Curie temperature T_c to zero [40, 41]. Uniaxial tensile strain applied to $SrTiO_3$ again causes it to become ferroelectric and suggests a small negative critical pressure of magnitude of the order of one kbar [42]. Measurements of the dielectric susceptibility under pressure [43–45] show a drastic suppression of the low temperature dielectric response as pressure is increased, matching the trend seen in the oxygen isotope doping studies which see a maximum in the size of χ at a substitution level of 36%, the same point where T_c tends to zero temperature. At this quantum critical point the frequency of the polar transverse optical phonon mode responsible for the ferroelectric ordering approaches zero at the Brillouin zone centre [42].

These and related studies, including those on superconductivity in doped $SrTiO_3$ [34, 46–60], shed light on the likely broad features of the temperature-quantum tuning parameter phase diagram of $SrTiO_3$. We now turn to our present findings that allow us to construct the first detailed phase diagram of this kind, with hydrostatic pressure as the chosen quantum tuning parameter. Importantly, our results enable us to identify the physical nature of the quantum paraelectric state at pressures above the critical pressure of the ferroelectric quantum critical point at low temperatures.

Results

Fig. 1 shows measurements of the dielectric susceptibility $\chi = \epsilon_r - 1$ of $SrTiO_3$ at ambient pressure and at increasing applied pressures. The ambient pressure data match the results of earlier work [28, 61] wherein the inverse susceptibility is linear at high temperatures matching the expected Curie-Weiss behaviour, be-
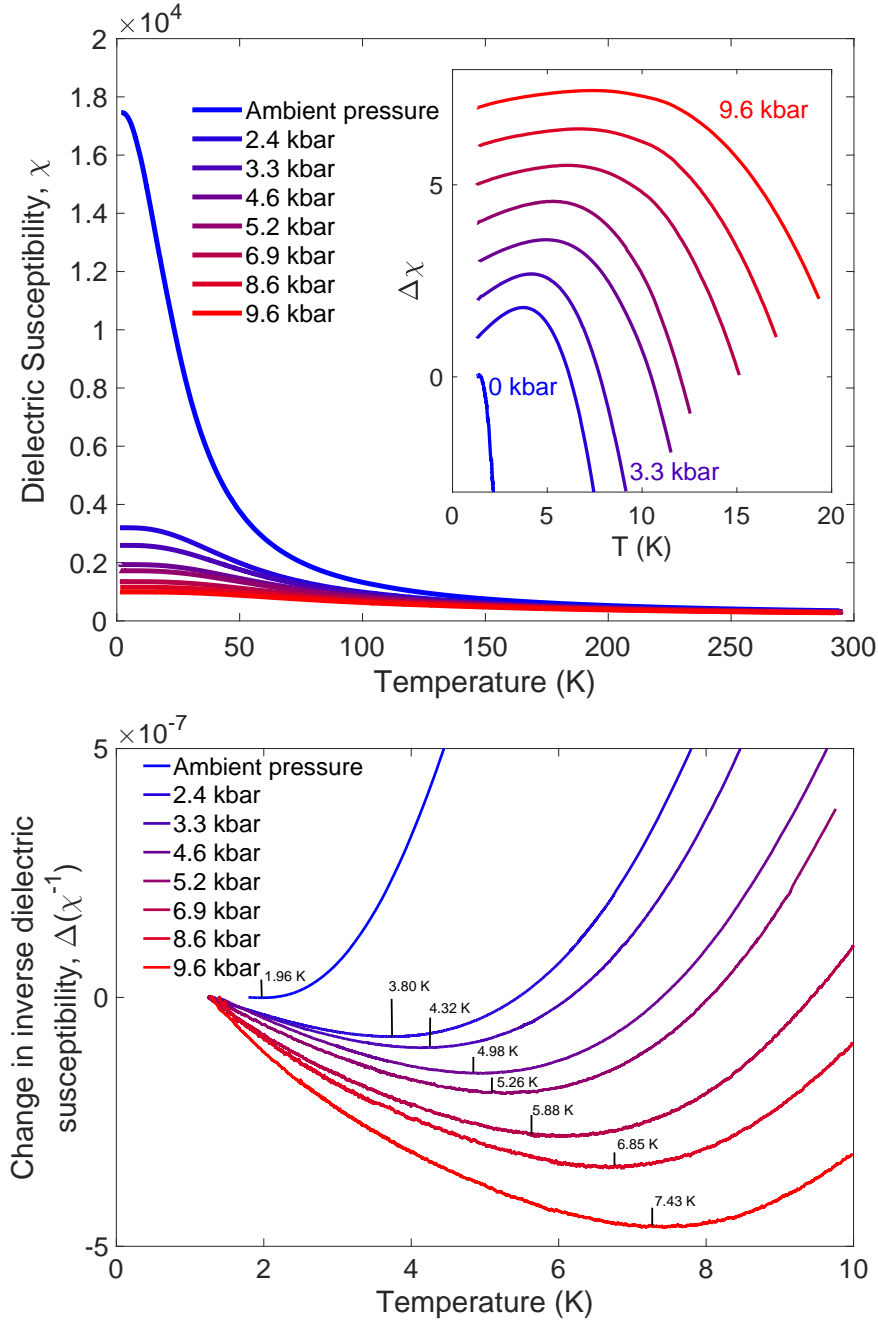
Figure 1: Upper plot - the dielectric susceptibility χ of SrTiO$_3$ plotted against temperature for applied pressures ranging from 0 (blue) to 9.6 (red) kbar. The magnitude of the dielectric susceptibility can be seen to be continuously reduced by the application of pressure. The inset shows the change in the low temperature values of χ from their lowest-temperature values; curves are offset for clarity. Importantly, χ initially rises with temperature and exhibits a peak that increases in position and magnitude with increasing pressure. For temperatures well below the peak temperature T^* the quantum paraelectric state involves a coherent coupling of polar and non-polar (acoustic) lattice vibrational modes. The lower plot shows the change in the inverse of χ from its lowest-temperature values for each pressure, where the feature is now a minimum.

fore crossing over to a quadratic power law dependence at lower temperatures due to quantum critical fluctuations. The low temperature dielectric susceptibility reaches a maximum at approximately 2 K with a value of around 20,000 before falling at even lower temperatures. Observed as a minimum in the inverse susceptibility, this effect is resolved here in much clearer detail than in earlier studies [28, 41] and is investigated as function of pressure. This minimum is seen to increase in depth with increasing pressure and its position, marked with arrows, moves up in temperature.

Moreover, we note from Fig. 1 that the initial negative variation of the inverse susceptibility, $\chi^{-1}(T)$, is quasi-linear, $(-T)$. We can reproduce this dependence in calculations made using a self-consistent Gaussian mean field model with coupled polar and non-polar modes, without the use of any free parameters, as shown in Fig. 2. We elaborate on these calculations and findings in the discussion section and in the Supplementary Material; our main finding is that the low-temperature data are best explained by the inclusion of a small density of quasi-static microdomains. These have little effect on the temperature and depth of the minimum, but even in tiny concentrations give rise to the quasi-linear low-temperature slope rather than the previously predicted $-T^4$ dependence.

Key features of the susceptibility are brought out in Fig. 3, which shows the pressure dependences of the $T \to 0$ K inverse susceptibility $\chi^{-1}(0)$, (main plot), the square of the position of the minimum T^* (upper inset) and the depth of the minimum $\Delta\chi^{-1}(T^*) = \chi^{-1}(0) - \chi^{-1}(T^*)$ (lower inset). All three curves extrapolate to zero at the same critical pressure, $p_c = -0.7$ kbar, i.e., at the ferroelectric quantum critical point, as suggested above. We see that $\chi^{-1}(0)$ varies linearly with $(p-p_c)$, T^* varies as the square root of $(p-p_c)$ and $\Delta\chi^{-1}(T^*)$ varies as $(p-p_c)$ to a power slightly greater than unity.

The variation of $\chi^{-1}(T)$ above a scale $T_{QC} > T^*$, which vanishes along with T^* at p_c, is found to be approximately quadratic, T^2, up to another scale T_{CL}, and is essentially linear in the classical regime above T_{CL} (Supplementary Material, SM, and Fig. 4). Pressure narrows the temperature window of the T^2 quantum critical regime while widening that of the regime described by the physics of quantum paraelectrics, $T < T_{CL}$, including the interesting regime below T^*. Combining the data for the pressure-dependent temperatures of the low-temperature minimum, T^*, (Fig. 1 and Fig. 3 upper inset) and the crossover temperatures from quantum paraelectric to quantum critical and from quantum critical to classical regimes, T_{QC} and T_{CL}, respectively, (Supplementary Material) with previous data on SrTi^{18}O$_3$ [41] that yields the Curie temperature, T$_c$, under pressure allows a full mapping of the temperature-pressure phase diagram of SrTiO$_3$, which is shown in Fig. 4.

Discussion

The main features of this phase diagram are consistent with the predictions of a 3-D self-consistent Gaussian mean field model, also known as the self-consistent phonon model [28], which assumes that $\chi^{-1}(0)$ is an analytic function of $(p - p_c)$ (in analogy to the assumption of analyticity in the Landau theory of phase transitions at finite temperatures) and that the temperature dependence $\chi^{-1}(T)$ is due to the thermal excitation of polar transverse optical modes whose gap, Δ, vanishes at the quantum critical point. The contribution of each mode depends on the inverse of their wavevector, so that in three dimensions at the quantum critical point one expects a contribution to $\chi^{-1}(T)$ of the form $(1/T)T^3$, or T^2, far below the relevant Debye temperature, T_D, and of the form T above a temperature, T_{CL}, calculated numerically to be a sizeable fraction of T_D. Away from the quantum critical point where Δ is finite the T^2 regime is cut off below a scale T_{QC} where the temperature dependence becomes exponentially weak as expected for activated phenomena. Since Δ^2 is expected to be proportional to $\chi^{-1}(0)$, which is proportional to $(p - p_c)$, we expect T_{QC} to be proportional to the square root of $(p - p_c)$, which is in keeping with observation (Fig. 4 and Supplementary Ma-
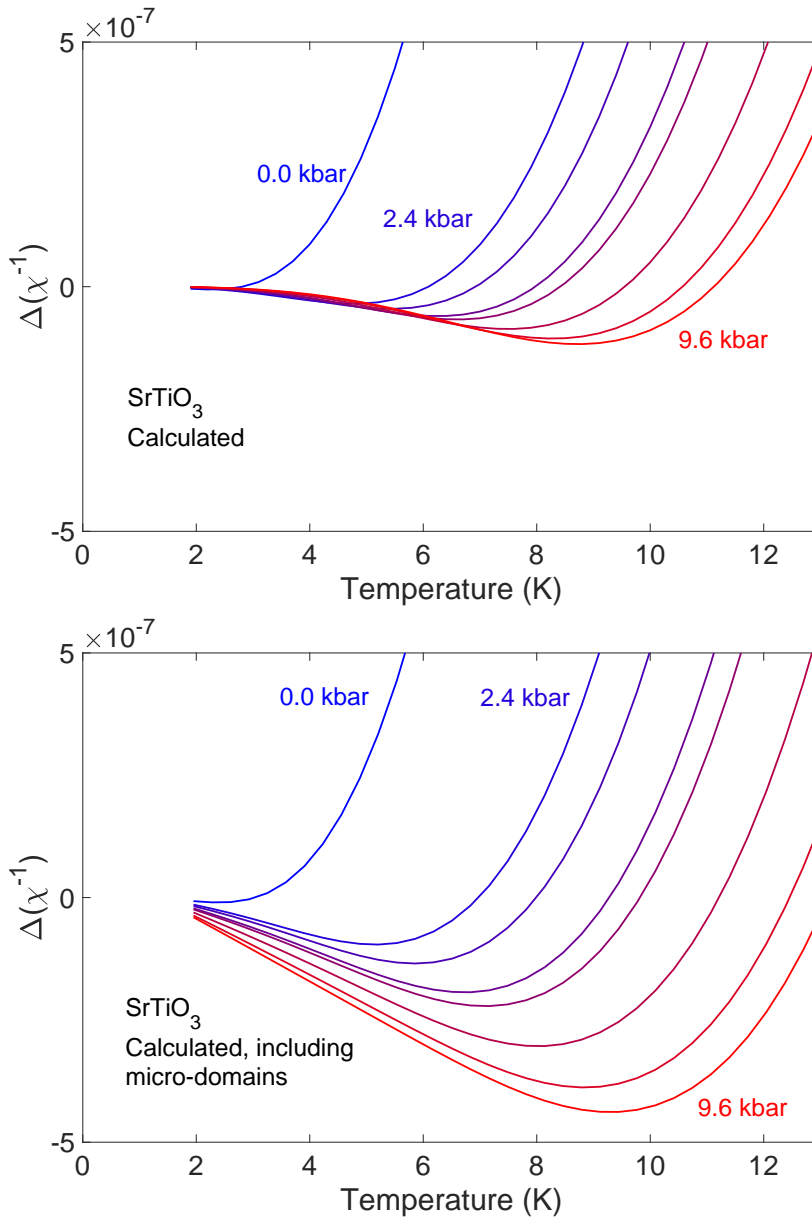
Figure 2: Calculated temperature variation of the inverse susceptibility at different applied pressures. Predictions of the self-consistent phonon model, including electrostrictive coupling, for the temperature dependence of $\Delta\chi^{-1}(T) = \chi^{-1}(T) - \chi^{-1}(T_{ref})$ for the applied pressures given in Fig. 1, with T_{ref} = 1.3 K. The upper and lower panels represent, respectively, the results excluding and including the contribution of micro-domains as discussed in the text and in the Supplementary Material. In both cases the minimum temperature T^* and depth are similar and grow with pressure approximately as $(p - p_c)^{1/2}$ and $(p - p_c)$, respectively, in agreement with observation (Figures 3 and S4). The inclusion of a contribution from a tiny concentration of quasi-static micro-domains, has only a modest effect on these properties, especially the minimum T^* vs $(p - p_c)^{1/2}$, but can drastically change the form of the temperature dependence of the inverse susceptibility at temperatures well below T^* (lower panel) to match the temperature dependence of the experimental data shown in Fig. 1. The details of the model and the model parameters employed in these calculations are given in the Supplementary Material.
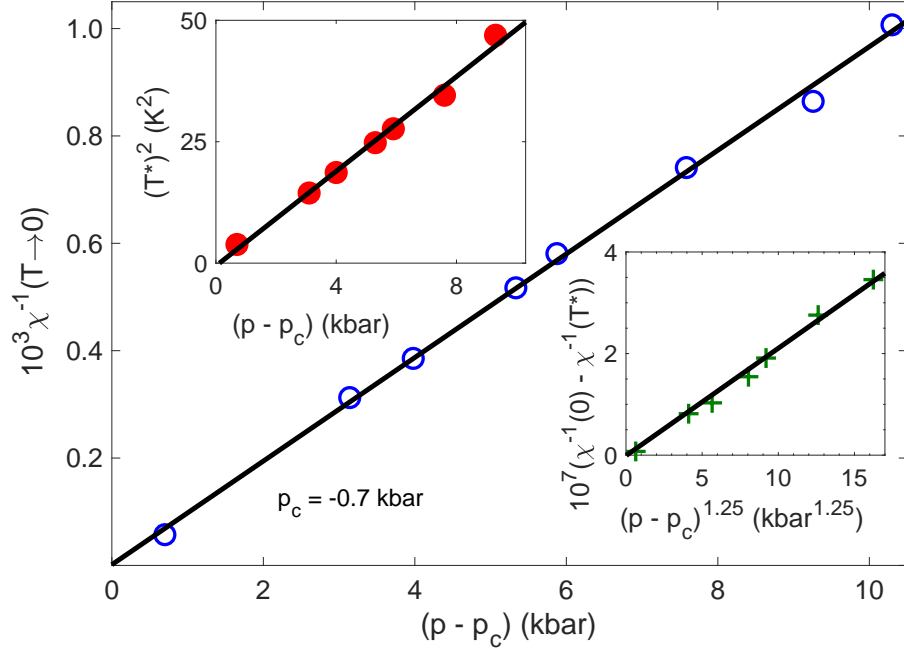
Figure 3: The low temperature inverse dielectric susceptibility $\chi^{-1}(0) = \chi^{-1}(T \to 0)$ as a function of applied pressure. We see that $\chi^{-1}(0)$ varies linearly with pressure and vanishes at the extrapolated critical pressure, p_c, of -0.7(1) kbar, defining the ferroelectric quantum critical point. The lower and upper insets show, respectively, the temperature dependences of the position of the minimum, T^*, and of the depth of the minimum, $\Delta\chi^{-1}(T^*)$. We see that the square of T^* is proportional to pressure and hence also to $\chi^{-1}(0)$. This is characteristic of the model of coupled polar and non-polar modes as described in the text.
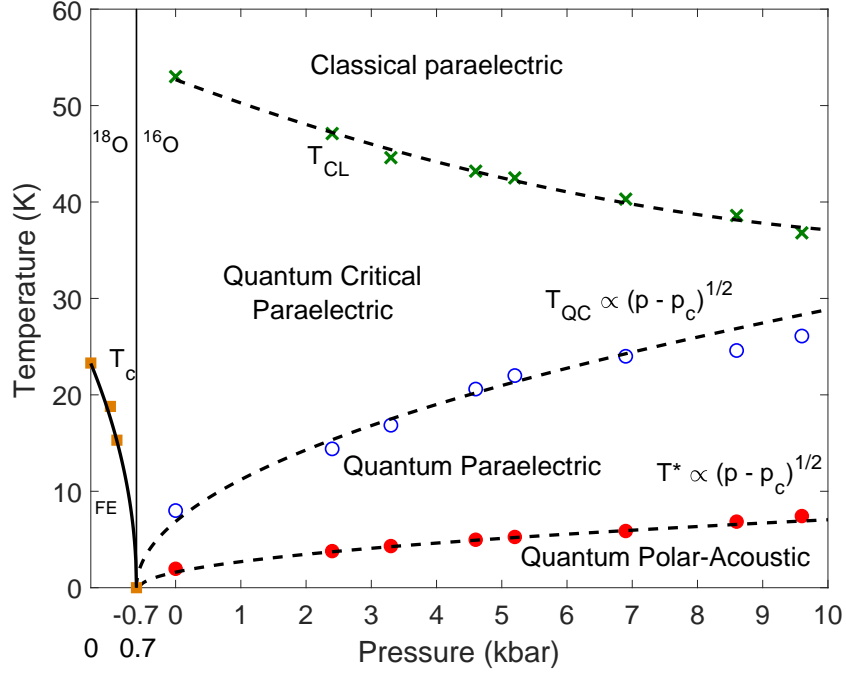
Figure 4: Phase diagram for SrTi^{16}O$_3$ from -0.7 to 10 kbar (right) and SrTi^{18}O$_3$ from 0 to 0.7 kbar (left), overlaid to match up the positions of proposed QCPs. Closed circles give the positions of the low temperature minimum, T^*, in χ^{-1} and open circles the crossover temperature, T_{QC} from the quantum paraelectric to quantum critical regimes. Dashed lines give fits of $(p - p_c)^{1/2}$ behaviour to both. Crosses show the crossover temperature, T_{CL}, between quantum critical and classical Curie-Weiss behaviour with a dotted guide to the eye. Squares and solid line show the ferroelectric Curie temperature, T_c, of SrTi^{18}O$_3$ taken from [41].

terial). Similar considerations lead us to expect T_c to also be proportional to the square root of $(p - p_c)$, which is consistent with previous studies in $SrTi^{18}O_3$. As shown previously for ambient pressure measurements, the self-consistent phonon model provides not only a qualitative but also quantitative understanding of the above behaviour in terms of independently measured model parameters.

However, the self-consistent phonon model in its simplest form fails to account for the low temperature behaviour presented here for $T < T^*$, which suggests that the quantum paraelectric state at low T is very different from the simple gapped state with activated behaviour conventionally invoked. In the remainder of the paper we consider alternative possible descriptions of this state and attempt to clarify its physical nature.

We discuss first the role of the coupling of the electric polarization with the non-polar lattice vibrations or acoustic phonons not included in the above self-consistent phonon model. As shown previously [16, 28] this coupling can account for the existence of a minimum of the inverse susceptibility with values of T^* and depth $\Delta\chi^{-1}(T^*)$ that are consistent with zero-temperature model parameters inferred from other measurements. Extending measurements to include the effect of pressure tuning, however, sheds light on a particularly distinctive prediction of the model, namely that the square of T^* should vary linearly with $\chi^{-1}(0)$ and hence vanish at the ferroelectric quantum critical point.

This prediction is strikingly supported by the data presented in the main plot and upper inset of Fig. 3, which show that both $(T^*)^2$ and $\chi^{-1}(0)$ vary linearly with $(p - p_c)$ and hence are proportional to each other. Moreover, as shown in the Supplementary Material, the absolute value of the slope of $(T^*)^2$ vs $\chi^{-1}(0)$ is consistent in order of magnitude with independently measured model parameters. Thus, at the critical pressure, p_c, $\chi^{-1}(T)$ has no minimum and is predicted to vary as the square of the temperature down to the lowest temperatures. For our model parameters the transition to the ferroelectric state is expected to be continuous at low temperatures, despite the polarization-acoustic phonons coupling (electrostriction) that is often expected to lead to first order transitions. This prediction appears to be in keeping with measurements to date in isotopically, chemically, pressure and strain tuned samples of $SrTiO_3$.

The polarization-acoustic phonon coupling model also predicts that the depth $\Delta\chi^{-1}(T^*)$ of the minimum should scale as $\chi^{-1}(0)$, which is partly supported from a comparison of the main plot and lower inset of Fig. 3. More importantly the polarization-phonon coupling model [16, 28] predicts that $\chi^{-1}(T)$ should vary as $(-T^4)$ below the inverse susceptibility minimum, which is in sharp disagreement with the negative quasi-linear dependence observed down to the lowest temperatures investigated [35]. The breakdown of the distinctive $(-T^4)$ prediction of the model is particularly striking at high pressures where temperature ranges up to two orders of magnitude below T^* can readily be accessed.

This dramatic departure from the prediction of the polarization-phonon coupling model leads us to consider alternative explanations for the susceptibility minimum. One such alternative explanation involves the combined effects of long-range dipolar interactions between elementary dipoles and the short range coupling of the polarization modes [62] (the mode-mode coupling) that can be represented within a Ginzburg-Landau expansion of the free energy, or the effective action in a more complete quantum description. It was suggested that this can lead to a susceptibility minimum qualitatively as predicted in the polarization-phonon coupling model, but crucially with a $(-T)$ rather than $(-T^4)$ temperature dependence of $\chi^{-1}(T)$ below T^*, qualitatively as observed.

However, on closer examination we find that this negative T-linear form only applies to a material such as $SrTiO_3$ at relatively high temperatures, indeed at scales above that of the longitudinal polar optical frequencies, which are far above the observed T^* in our experiments. In the temperature range below of the order of 10 K the dipole-dipole interaction model predicts an exponentially weak rather than a $(-T)$ temperature dependence of $\chi^{-1}(T)$, which is in sharp disagreement with observation. For this and other reasons the dipole-dipole interaction model appears to be untenable at least for the case of $SrTiO_3$ and does not explain the

pressure dependence of T^* and of the depth of the minimum. It is also unlikely to operate in other materials where the minimum has been observed, such as TSCC, which have ultra-weak, nearly neutral, dipoles [29].

Another alternative explanation involves a possible refinement of the polarization-acoustic phonon coupling model, which, as already noted, predicts correctly the linear relationship between $(T^*)^2$ and $\chi^{-1}(0)$. The chief weakness of this model, namely the predicted $(-T^4)$ temperature dependence of $\chi^{-1}(T)$ below T^*, compared with the observed $(-T)$ form, might be corrected via the inclusion of a low density of quasi-static modes of the lattice that can be treated effectively by classical statistics. To account for the observed $(-T)$ temperature dependence, the density of such modes need only be in the parts per million range (Supplementary Material), and normally outside the detection range of most probes. For example, the contribution to the specific heat capacity would be a small and virtually undetectable constant offset.

Interestingly, numerical analyses show that the inclusion of such a low density of slow classical modes, along with the acoustic phonons, leaves the linear relationship between $(T^*)^2$ and $\chi^{-1}(0)$ largely unchanged. This suggests that the observed $(-T)$ variation of $\chi^{-1}(T)$ is not inconsistent with the observed linear variation of $(T^*)^2$ vs $\chi^{-1}(0)$. In contrast, however, the dependence of the depth $\Delta\chi^{-1}(T^*)$ on $\chi^{-1}(0)$ is noticeably affected by the low density of slow modes and this too is qualitatively in agreement with observation (main plot and lower inset of Fig. 3, and Supplementary Material).

We now consider one possible origin of the proposed quasi-static modes. The polarization-acoustic phonon coupling model discussed thus far takes into account only the coupling of the polarization to the lattice density or to the volume strain. It has been shown that the coupling to non-uniform strain can in principle give rise to long-range strain-mediated interactions between the polarization modes (i.e., long-range mode-mode coupling). These long-range interactions are capable of producing micro-domain structures in the polarization field under certain conditions [30, 63], which may be expected to exhibit slow temporal fluctuations and, correspondingly, classical behaviour even at temperatures well below T^*. Independent evidence for the possible existence of inhomogeneities comes from a number of studies [64] and, for example, from recent measurements of the thermal conductivity [65], which reveal a surprisingly short mean-free path of phonons even in the millikelvin temperature range and in high purity single crystals of SrTiO$_3$.

We therefore conclude that the susceptibility minimum in SrTiO$_3$ can be understood largely in terms of the polarization-acoustic phonon coupling model including a contribution from a minute density of slow lattice modes, which may owe their existence to the long-range strain induced interactions that are neglected in the polarization-phonon coupling model in its simplest form. An alternative explanation for the susceptibility minimum in terms of the anharmonic effects of the long-range dipole-dipole interaction is found to be untenable at least for the case of SrTiO$_3$. Thus, we may describe the quantum paraelectric state below T^* as a state in which the polarization field and the non-polar lattice field are strongly hybridized, with the emergence at still lower temperatures of slowly fluctuating micro-domains, or instantons. This is in sharp contrast to the conventional picture in which a ferroelectric quantum phase transition separates a ferroelectric state from an unhybridized paraelectric state characterized by an activated form of the temperature dependence of the inverse susceptibility.

References

[1] J.A. Hertz. Quantum critical phenomena. *Phys. Rev. B*, 14(3):1165–1184, 1976.

[2] A.J. Millis. Effect of a non-zero temperature on quantum critical points in itinerant fermion systems. *Phys. Rev. B*, 48(10):7183–7196, 1993.

[3] P.W. Anderson. In praise of unstable fixed points: the way things actually work. *Physica B: Condensed Matter*, 318(1):28–32, 2002.

[4] G.G. Lonzarich. *The Magnetic Electron*. Cambridge University Press, 1997.

[5] P. Coleman and A.J. Schofield. Quantum criticality. *Nature*, 433(7023):226–229, 2005.

[6] A. Kopp and S. Chakravarty. Criticality in correlated quantum matter. *Nature Physics*, 1(1):53–56, 2005.

[7] P.C. Canfield. Fishing the Fermi sea. *Nature Physics*, 4(3):167–169, 2008.

[8] P. Monthoux, D. Pines, and G.G. Lonzarich. Superconductivity without phonons. *Nature*, 450(7173):1177–1183, 2007.

[9] Subir Sachdev. *Quantum phase transitions*. Cambridge university press, 2011.

[10] H. v. Löhneysen, A. Rosch, M. Vojta, and P. Wölfle. Fermi-liquid instabilities at magnetic quantum phase transitions. *Reviews of Modern Physics*, 79(3):1015–1075, Aug 2007.

[11] F.M. Grosche, I.R. Walker, S.R. Julian, N.D. Mathur, D.M. Freye, M.J. Steiner, and G.G. Lonzarich. Superconductivity on the threshold of magnetism in CePd$_2$Si$_2$ and CeIn$_3$. *Journal of Physics: Condensed Matter*, 13(12):2845–2860, Mar 2001.

[12] S.S. Saxena, P. Agarwal, K. Ahilan, F.M. Grosche, R.K.W. Haselwimmer, M.J. Steiner, E. Pugh, I.R. Walker, S.R. Julian, P. Monthoux, and et al. Superconductivity on the border of itinerant-electron ferromagnetism in UGe$_2$. *Nature*, 406(6796):587–592, 2000.

[13] M. Lee, W. Kang, Y. Onose, Y. Tokura, and N.P. Ong. Unusual Hall effect anomaly in MnSi under pressure. *Physical Review Letters*, 102(18), 2009.

[14] G.G. Lonzarich. Quantum criticality: Magnetic quantum liquid enigma. *Nature Physics*, 1(1):11–12, 2005.

[15] A.B. Rechester. Contribution to the theory of second-order phase transitions at low temperatures. *Soviet Journal of Experimental and Theoretical Physics*, 33:423, 1971.

[16] D.E. Khmel'nitskiĭ and V.L. Schneerson. Low-temperature displacement-type phase transition in crystals. *Soviet Physics - Solid State*, 13:832–841, 1971.

[17] D.E. Khmel'nitskiĭ and V.L. Shneerson. Phase transitions of the displacement type in crystals at very low temperatures. *Soviet Journal of Experimental and Theoretical Physics*, 37:164, Jul 1973.

[18] U.T. Höchli and L.A. Boatner. Quantum ferroelectricity in $K_{1-x}Na_xTaO_3$ and $KTa_{1-y}Nb_yO_3$. *Physical Review B*, 20(1):266–275, 1979.

[19] J.G. Bednorz and K.A. Müller. $Sr_{1-x}Ca_xTiO_3$: An XY quantum ferroelectric with transition to randomness. *Physical Review Letters*, 52(25):2289–2292, 1984.

[20] O.E. Kvyatkovskii. Quantum effects in incipient and low-temperature ferroelectrics (a review). *Physics of the Solid State*, 43(8):1401–1419, 2001.

[21] R. Roussev and A.J. Millis. Theory of the quantum paraelectric-ferroelectric transition. *Physical Review B*, 67(1), 2003.

[22] E.L. Venturini, G.A. Samara, M. Itoh, and R. Wang. Pressure as a probe of the physics of ^{18}O-substituted $SrTiO_3$. *Physical Review B*, 69(18), 2004.

[23] H. Wu and W. Z. Shen. Dielectric and pyroelectric properties of $Ba_xSr_{1-x}TiO_3$: Quantum effect and phase transition. *Physical Review B*, 73(9), 2006.

[24] N. Das and S.G. Mishra. Fluctuations and criticality in quantum paraelectrics. *Journal of Physics: Condensed Matter*, 21(9):095901, 2009.

[25] L. Pálová, P. Chandra, and P. Coleman. Quantum critical paraelectrics and the Casimir effect in time. *Physical Review B*, 79(7), Feb 2009.

[26] S.E. Rowley. *Quantum phase transitions in ferroelectrics*. PhD thesis, University of Cambridge, 2010.

[27] S.E. Rowley, R. Smith, M. Dean, L. Spalek, M. Sutherland, M. Saxena, P. Alireza, C. Ko, C. Liu, E. Pugh, S. Sebastian, and G.G. Lonzarich. Ferromagnetic and ferroelectric quantum phase transitions. *Physica Status Solidi (b)*, 247(3):469–475, 2010.

[28] S.E. Rowley, L.J. Spalek, R.P. Smith, M.P.M. Dean, M. Itoh, J.F. Scott, G.G. Lonzarich, and S.S. Saxena. Ferroelectric quantum criticality. *Nat Phys*, 10(5):367–372, 2014.

[29] S.E. Rowley, M. Hadjimichael, M.N. Ali, Y.C. Durmaz, J.C. Lashley, R.J. Cava, and J.F. Scott. Quantum criticality in a uniaxial organic ferroelectric. *J. Phys.: Condens. Matter*, 27(39):395901, 2015.

[30] S.E. Rowley and G.G. Lonzarich. Ferroelectrics in a twist. *Nature Physics*, 10(12):907–908, 2014.

[31] S. Horiuchi, K. Kobayashi, R. Kumai, N. Minami, F. Kagawa, and Y. Tokura. Quantum ferroelectricity in charge-transfer complex crystals. *Nature Communications*, 6(1), 2015.

[32] S.E. Rowley, Y.S. Chai, S.P. Shen, Y. Sun, A.T. Jones, B.E. Watts, and J.F. Scott. Uniaxial ferroelectric quantum criticality in multiferroic hexaferrites $BaFe_{12}O_{19}$ and $SrFe_{12}O_{19}$. *Scientific Reports*, 6:25724, 2016.

[33] P. Chandra, G.G. Lonzarich, S.E. Rowley, and J.F. Scott. Prospects and applications near ferroelectric quantum phase transitions: a key issues review. *Reports on Progress in Physics*, 80(11):112502, 2017.

[34] C.W. Rischau, X. Lin, C.P. Grams, D. Finck, S. Harms, J. Engelmayer, T. Lorenz, Y. Gallais, B. Fauqué, J. Hemberger, and K. Behnia. A ferroelectric quantum phase transition inside the superconducting dome of $Sr_{1-x}Ca_xTiO_{3-\delta}$. *Nature Physics*, 13(7):643–648, 2017.

[35] M.J. Coak. *Quantum tuning and emergent phases in charge and spin ordered materials*. PhD thesis, University of Cambridge, 2017.

[36] M.E. Lines and A.M. Glass. *Principles and applications of ferroelectrics and related materials*. Oxford university press, 1977.

[37] W. A. Atkinson, P. Lafleur, and A. Raslan. Influence of the ferroelectric quantum critical point on $SrTiO_3$ interfaces. *Physical Review B*, 95(5), Feb 2017.

[38] C. Tinsman, G. Li, C. Su, T. Asaba, B. Lawson, F. Yu, and L. Li. Probing the thermal Hall effect using miniature capacitive strontium titanate thermometry. *Applied Physics Letters*, 108(26):261905, 2016.

[39] K.A. Müller, W. Berlinger, and E. Tosatti. Indication for a novel phase in the quantum paraelectric regime of $SrTiO_3$. *Z. Physik B - Condensed Matter*, 84(2):277–283, Jun 1991.

[40] M. Itoh and R. Wang. Quantum ferroelectricity in $SrTiO_3$ induced by oxygen isotope exchange. *Applied Physics Letters*, 76(2):221, 2000.

[41] R. Wang, N. Sakamoto, and M. Itoh. Effects of pressure on the dielectric properties of $SrTi^{18}O_3$ and $SrTi^{16}O_3$ single crystals. *Physical Review B*, 62(6):R3577–R3580, Aug 2000.

[42] H. Uwe and T. Sakudo. Stress-induced ferroelectricity and soft phonon modes in $SrTiO_3$. *Physical Review B*, 13(1):271–286, 1976.

[43] E. Hegenbarth and C. Frenzel. The pressure dependence of the dielectric constants of $SrTiO_3$ and $Ba_{0.05}Sr_{0.95}TiO_3$ at low temperatures. *Cryogenics*, 7(1-4):331–335, 1967.

[44] C. Frenzel and E. Hegenbarth. The influence of hydrostatic pressure on the field-induced dielectric constant maxima of $SrTiO_3$. *Phys. Stat. Sol. (a)*, 23(2):517–521, 1974.

[45] B. Pietrass and E. Hegenbarth. The influence of pressure on phase transitions at low temperatures: $SrTiO_3$ and $(Ba_xSr_{1-x})TiO_3$. *J Low Temp Phys*, 7(3-4):201–209, 1972.

[46] J. F. Schooley, W. R. Hosler, and Marvin L. Cohen. Superconductivity in semiconducting $SrTiO_3$. *Physical Review Letters*, 12(17):474–475, 1964.

[47] D. van der Marel, J. L. M. van Mechelen, and I. I. Mazin. Common fermi-liquid origin of T^2 resistivity and superconductivity in *n*-type $SrTiO_3$. *Physical Review B*, 84(20), 2011.

[48] J.F. Scott, E.K.H. Salje, and M.A. Carpenter. Domain wall damping and elastic softening in $SrTiO_3$: Evidence for polar twin walls. *Phys. Rev. Lett.*, 109(18), 2012.

[49] A. Lopez-Bezanilla, P. Ganesh, and P.B. Littlewood. Research update: Plentiful magnetic moments in oxygen deficient $SrTiO_3$. *APL Materials*, 3(10):100701, 2015.

[50] S.E. Rowley, C. Enderlein, J. Ferreira de Oliveira, D.A. Tompsett, E. Baggio Saitovitch, S.S. Saxena, and G.G. Lonzarich. Superconductivity in the vicinity of a ferroelectric quantum phase transition. *ArXiv*, (1801.08121v2), 2018.

[51] X. Lin, Z. Zhu, B. Fauqué, and K. Behnia. Fermi surface of the most dilute superconductor. *Physical Review X*, 3(2), 2013.

[52] K. Ueno, S. Nakamura, H. Shimotani, A. Ohtomo, N. Kimura, T. Nojima, H. Aoki, Y. Iwasa, and M. Kawasaki. Electric-field-induced superconductivity in an insulator. *Nature Materials*, 7(11):855–858, 2008.

[53] R.M. Fernandes, J.T. Haraldsen, P. Wölfle, and A.V. Balatsky. Two-band superconductivity in doped SrTiO₃ films and interfaces. *Physical Review B*, 87(1), 2013.

[54] S.N. Klimin, J.Tempere, J.T. Devreese, and D. van der Marel. Interface superconductivity in LaAlO₃-SrTiO₃ heterostructures. *Physical Review B*, 89(18), 2014.

[55] X. Lin, G. Bridoux, A. Gourgout, G. Seyfarth, S. Krämer, M. Nardone, B. Fauqué, and K. Behnia. Critical doping for the onset of a two-band superconducting ground state in SrTiO$_{3-\delta}$. *Physical Review Letters*, 112(20), 2014.

[56] J.M. Edge, Y. Kedem, U. Aschauer, N.A. Spaldin, and A.V. Balatsky. Quantum critical origin of the superconducting dome in SrTiO₃. *Physical Review Letters*, 115(24), 2015.

[57] J. Ruhman and P.A. Lee. Superconductivity at very low density: The case of strontium titanate. *Physical Review B*, 94(22), 2016.

[58] A.V. Chubukov, I. Eremin, and D.V. Efremov. Superconductivity versus bound-state formation in a two-band superconductor with small Fermi energy: Applications to Fe pnictides/chalcogenides and doped SrTiO₃. *Physical Review B*, 93(17), 2016.

[59] L.P. Gor'kov. Phonon mechanism in the most dilute superconductor n-type SrTiO₃. *Proceedings of the National Academy of Sciences*, 113(17):4646–4651, 2016.

[60] A. Stucky, G.W. Scheerer, Z. Ren, D. Jaccard, J.-M. Poumirol, C. Barreteau, E. Giannini, and D. van der Marel. Isotope effect in superconducting n-doped SrTiO₃. *Scientific Reports*, 6(1), 2016.

[61] K.A. Müller and H. Burkard. SrTiO₃ : An intrinsic quantum paraelectric below 4 K. *Phys. Rev. B*, 19(7):3593–3602, Apr 1979.

[62] G.J. Conduit and B.D. Simons. Theory of quantum paraelectrics and the metaelectric transition. *Physical Review B*, 81(2), 2010.

[63] R.T. Brierley and P.B. Littlewood. Domain wall fluctuations in ferroelectrics coupled to strain. *Physical Review B*, 89(18), 2014.

[64] E.K.H. Salje, O. Aktas, M.A. Carpenter, V.V. Laguta, and J.F. Scott. Domains within domains and walls within walls: Evidence for polar domains in cryogenic SrTiO₃. *Physical Review Letters*, 111(24), 2013.

[65] V. Martelli, J.L. Jiménez, M. Continentino, E. Baggio-Saitovitch, and K. Behnia. Thermal transport and phonon hydrodynamics in strontium titanate. *Physical Review Letters*, 120(12), 2018.

Supplementary Material

Methods

High precision capacitance measurements were carried out on single crystal samples of SrTiO₃ from Crystal GmbH with gold electrodes vacuum evaporated onto the surfaces in a parallel-plate capacitor geometry. Measurements under hydrostatic pressure conditions were made possible by the development, in collaboration with CamCool Research Ltd, of a piston-cylinder clamp cell with miniature shielded coaxial cables running into the sample region and electrically isolated from the cell body. This eliminates stray capacitances from the wiring and allows pF capacitance signals to be measured with stabilities of up to 10^{-18} F, a few parts in a billion. The shield conductors of the coaxial cables were joined together at the
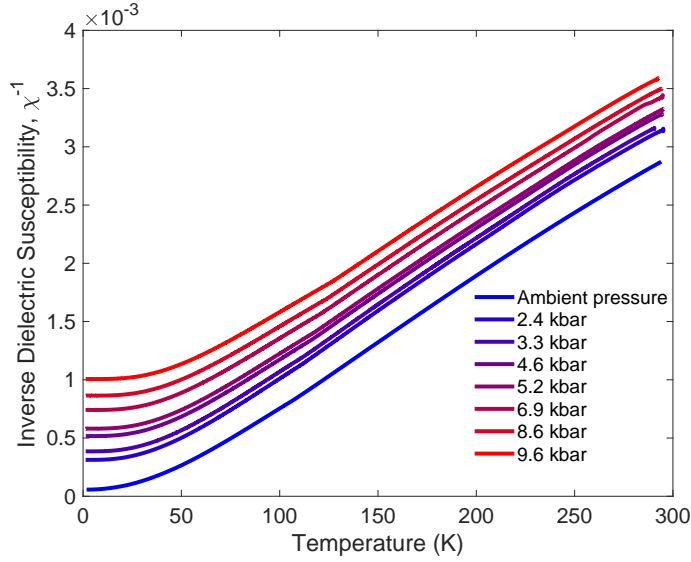
Figure S1: Inverse dielectric susceptibility χ^{-1} of SrTiO₃ plotted against temperature for applied pressures ranging from 0 (blue) to 9.6 (red) kbar.

sample position and at the measurement instrument in the standard 2-point capacitance setup. The pressure transmitting medium was Daphne Oil 7373 and pressure values, determined from the superconducting transition temperature of a tin manometer, were estimated with an accuracy of 0.5 kbar. An Andeen-Hagerling 2550A capacitance bridge was used, with an excitation amplitude voltage of 0.1 V at a fixed frequency of 1 kHz applied to the sample. The sample thickness, corresponding to capacitor plate separation, was 0.5 mm. Most measurements were taken on a modified 1 K Dipper cryostat from ICE Oxford, allowing continuous stable temperature control down to 1.2 K. Typical heating or cooling rates were held at 0.01 K per minute to allow the large thermal mass of the pressure cell to thermally equilibrate; temperature errors are of the order 10 mK at low temperature. Typical results of our measurements are shown in Figures S1-3 and Figure 1 in the main body of the paper.

Self Consistent Phonon Theory

The calculations of the dielectric susceptibility, $\chi(T) = \varepsilon_r(T) - 1$, were carried out in terms of the self-consistent phonon model for a simple displacive ferroelectric in three dimensions, see Refs [26, 28] and references therein. We consider first the effects of the self interaction of the electric polarization field as represented by a local quartic term in the effective Lagrangian density, expressed as a function of the polarization field and its temporal and spatial gradients. In the mean field approximation for the self-interaction the polarization correlation wavevector, or inverse correlation length, $\kappa(T)$, is determined from the self-consistent equation

$$\kappa^2(T) = \kappa^2(0) + \zeta \int dq \, q^2 \left[\sum_n \frac{T}{\kappa^2(T) + q^2 + \omega_n^2} - \frac{1}{2\pi} \int \frac{d\omega}{\kappa^2(0) + q^2 + \omega^2} \right] \quad (1)$$

where the wavevectors q, $\kappa(T)$ and $\kappa(0) = \kappa(T = 0)$ are in units of the relevant Debye wavevector Λ, T is in units of the relevant Debye temperature θ and $\omega_n = 2\pi nT$, where n is an integer. The cut-offs in wavevector and frequency are taken to be unity in these units (i.e., $0 < q < 1$ and $-1 < \omega < 1$). The dimensionless correlation wavevector $\kappa(T)$ and the dimensionless coupling parameter ζ are given, in terms of the model parameters defined in the next section and in Ref
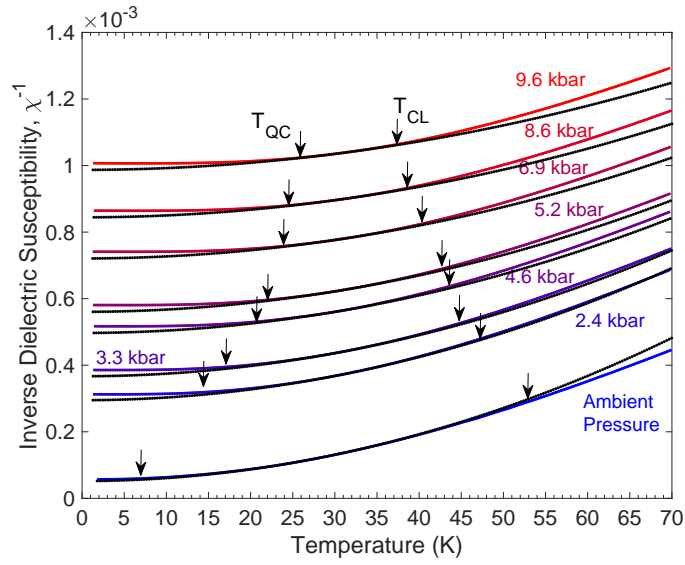
Figure S2: The measured values of χ^{-1} as a function of temperature at different fixed pressures (shown as coloured dots) were fitted to an equation of the form $\chi^{-1} = A + BT^2$ over the temperature range 0 to 70 K (A and B are fitting parameters). The fitted curves are shown as black dotted lines for each pressure. The lower and upper cross-over temperatures T_{QC} and T_{CL}, marked with arrows, were defined as occurring when the experimental value of χ^{-1} deviated from the fitted value by 1%.
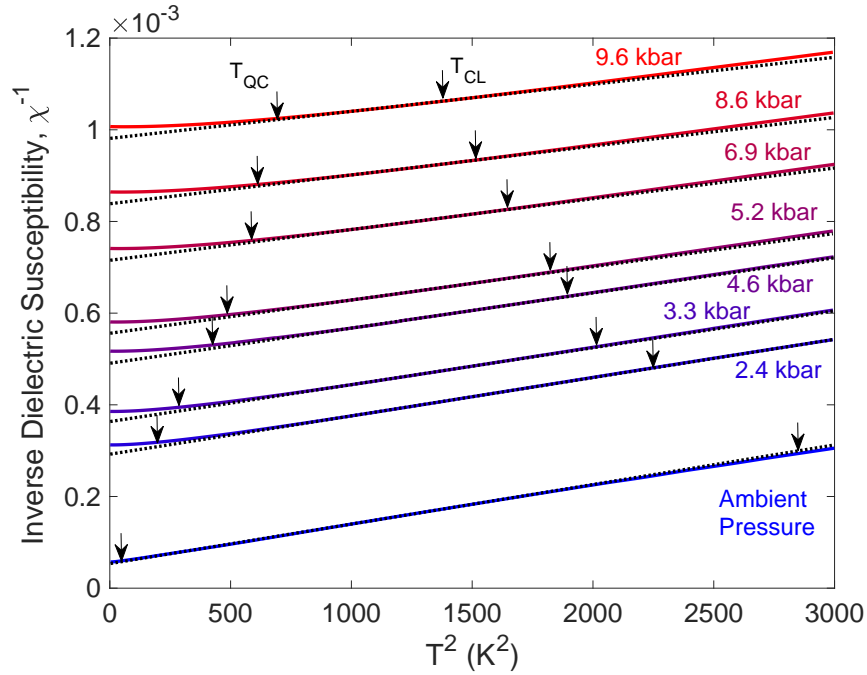

Figure S3: Inverse dielectric susceptibility χ^{-1} of SrTiO$_3$ plotted against the square of temperature for applied pressures ranging from 0 (blue) to 9.6 (red) kbar. The regions where the data are linear, indicating a T^2 temperature dependence, lie between the characteristic crossover temperatures T_{QC} and T_{CL}, marked with arrows. T_{QC} and T_{CL}, described more in the main text, were determined as the temperatures at which the measured value of χ^{-1} deviated from the fitted value of χ^{-1} by 1%.

15

[28], by

$$\kappa^2(T) = \frac{\Delta^2 \chi(0)}{v^2 \Lambda^2 \chi(T)} \tag{2}$$

and

$$\zeta = \frac{5\varepsilon_0 \hbar b \Delta^4 \chi^2(0)}{3\pi^2 v^3} \tag{3}$$

where $\chi(0) = \chi(T = 0)$, Δ and v define the "$T = 0$" spectrum of the critical transverse optical modes and b is the coefficient of the anharmonic term in the equation of state assumed to have the analytic form $\varepsilon_0 E = P/\chi(T) + bP^3$, where E is the electric field that stabilizes the polarization P. Thus $\kappa^2(T)$ is a dimensionless measure of the inverse dielectric susceptibility. We also note that the square of the gap of the spectrum of critical transverse optical modes is expected to be proportional to the inverse susceptibility, so that $\Delta^2(T) = \chi^{-1}(T)\Delta^2/\chi^{-1}(0)$, where $\Delta = \Delta(0)$.

The coupling between the critical transverse optic mode and the acoustic mode, or more precisely the volume strain, leads to a further correction to $\kappa^2(T)$ of the form

$$\delta\kappa^2(T) = -\lambda \int dq \, q^4 \left[\sum_n \frac{T}{(\kappa^2(T) + q^2 + \omega_n^2)(q^2 + \eta^2\omega_n^2)} \right.$$
$$\left. -\frac{1}{2\pi} \int \frac{d\omega}{(\kappa^2(0) + q^2 + \omega^2)(q^2 + \eta^2\omega_n^2)} \right] \tag{4}$$

where η is the ratio of the velocity of critical transverse optical modes to the velocity of the acoustic mode and λ is a dimensionless electrostrictive coupling constant. We have estimated the latter via the strain dependence of the energy gap of the order parameter mode [28] that suggests

$$\lambda \approx \frac{3K\zeta}{20\varepsilon_0 b p_c^2 \chi^2(0)} \tag{5}$$

where ζ is the dimensionless parameter defined in Eq. 3, K is the bulk modulus and p_c is the critical pressure (negative for SrTiO$_3$) where the $T = 0$ K correlation wavevector is expected to vanish. We note that the electrostrictive effect is also expected to make a negative contribution to the mode-coupling parameter, b, and lead potentially to a first order transition. Numerical estimates suggest, however, that the transition should remain second order under our experimental conditions in agreement with measurements down to 0.3 K in SrTiO$_3$ [28]. Nonetheless, as one approaches even closer to the quantum critical point than explored in our experiments, a sign change in b may occur.

We note that in the limit where κ^2 is comparable to or greater than q^2 in the above equations (for all $q < \Lambda$), the above model in the absence of the electrostrictive effect and self-consistency reduces to the Barrett model. The latter cannot describe the quantum critical regime where the frequencies of the modes are strongly wavevector and temperature dependent, nor below the crossover temperature T^* in general where the electrostrictive effect changes the qualitative nature of the quantum paraelectric state.

The prediction of the above model (defined by Equations 1-5) for the temperature dependence of the susceptibility at a series of applied hydrostatic pressures for model parameters relevant to SrTiO$_3$ (next section) is shown in Figure 2a in the main body of the paper. For calculations at finite pressures the ambient pressure parameters $\chi^{-1}(0)$ and Δ are replaced, respectively, by $\chi^{-1}(0)(1 - p/p_c)$ and $\Delta(1 - p/p_c)^{1/2}$, while b and v are held constant. The results exhibit a minimum arising from the electrostrictive coupling with the minimum temperature T^* and depth $\Delta\chi^{-1}(T^*)$ that decrease with decreasing pressure and vanish at the ferroelectric quantum critical point at $p_c = -0.7$ kbar. As shown in Figures S4a and

S4b the model predicts that $(T^*)^2$ and the depth $\Delta\chi^{-1}(T^*)$ should both be proportional to $(p - p_c)$. The former prediction, in particular, is in excellent agreement with experiment (Figure 3 in the main body of the paper). However, the electrostrictive coupling model also predicts a $(-T^4)$ temperature dependence of $\Delta\chi^{-1}(T^*)$ well below T^*, which is inconsistent with the negative quasi-linear variation observed (cf. Figures 1 and 2 in the main body of the paper).

In an effort to understand this unexpected behaviour, we have also considered the possible roles of the long-range dipole-dipole interaction and of quasi-static inhomogeneities of the lattice or micro domains predicted to arise from anisotropic couplings (including wavevector dependence) of the strain and electric polarization fields. The main effect of the dipolar interaction is to modify a degeneracy factor defining the dimensionless self-interaction coupling parameter already included in the expression for ζ given in Equation (3). Additional predicted consequences of the dipolar interaction are found not to be relevant to SrTiO$_3$ at low temperatures as discussed in the main body of the paper.

We have considered the possible electrostrictive effects of micro domains [30, 63, 64] by including an additional term on the right hand side of Equation (4) in which the acoustic phonon spectrum is replaced by an Einstein spectrum with a gap Δ_E. The weight of the additional term is taken to be the relative concentration, c_E, of the micro-domains in the system. In the limit $\Delta_E << \Delta$ the micro-domain contribution, even with a very tiny concentration c_E, can greatly alter the temperature dependence of $\chi^{-1}(T)$ below the scale of T^* - Figures 2a and 2b in the main body of the paper. Importantly, this contribution can in principle account for the negative quasi-linear low temperature dependence of the inverse susceptibility as well as the linear relation between $(T^*)^2$ and $(p - p_c)$, which interestingly turns out to be little affected by the micro-domain contribution for model parameters consistent with observation (cf. Figure 2 in the main body of the paper). We note that we have used the term micro-domain to potentially represent a number of different types of micro textures with slow dynamics [30, 48, 63, 64] that can be represented phenomenologically in a similar manner.

Model Parameters for SrTiO$_3$

The starting self-consistent phonon model for a displacive ferroelectric is defined mainly in terms of four temperature independent parameters, which we take to be $\chi^{-1}(0)$, b, Δ, and v. The parameters $\chi^{-1}(0)$ and b were obtained from the intercept and slope, respectively, of plots of $\varepsilon_0 E/P$ vs P^2 at 0.3 K [26], where E is the electric field (0 to 15 kV/cm in our measurements) and P is the electric polarization, given an equation of state of the analytic form $\varepsilon_0 E/P = \chi^{-1}(0) + bP^2$. The parameters v and Δ were determined by comparing the data from inelastic neutron and Raman scattering experiments at 4 K to an equation of the form $\omega_q^2 = \Delta^2 + v^2 q^2$, which defines the low q and low T dispersion in the paraelectric state of the transverse-optic phonons that are the soft modes of the incipient ferroelectric state (see Ref [28] and references therein). Values for $\chi^{-1}(0)$, b, and v for SrTiO$_3$ in the low temperature limit used in the calculations were set equal to $2 \times 10^4 (= \varepsilon_r(0)–1)$, $0.07\ C^2m^4$ and $8100\ ms^{-1}$, respectively [28]. The results of calculations presented are based on three values of the gap $\hbar\Delta/k_B$ equal to 6, 12 and 24 K. The intermediate value was used for the calculations presented in Figure 2 in the main body of the paper. This is somewhat lower than but of the same order of magnitude as that estimated by inelastic neutron scattering.

We note that the square of the gap is expected to be proportional to the inverse susceptibility, so that $\Delta^2(T) = \chi^{-1}(T)\Delta^2/\chi^{-1}(0)$, where $\Delta = \Delta(0)$, and that v reduces to the speed of sound of the critical transverse optical modes when the gap vanishes. The relatively small value of Δ implies that SrTiO$_3$ is close to a displacive ferroelectric quantum critical point at ambient pressure. For a Debye wavevector $\Lambda = 0.08$ nm, the dimensionless self-interaction coupling constant ζ defined in Eq S3 is approximately 0.8.

Also we have taken $\eta = 2$, $\theta = 600$ K, $\Delta = 12$ K, $p_c = -0.7$ kbar and $K =$
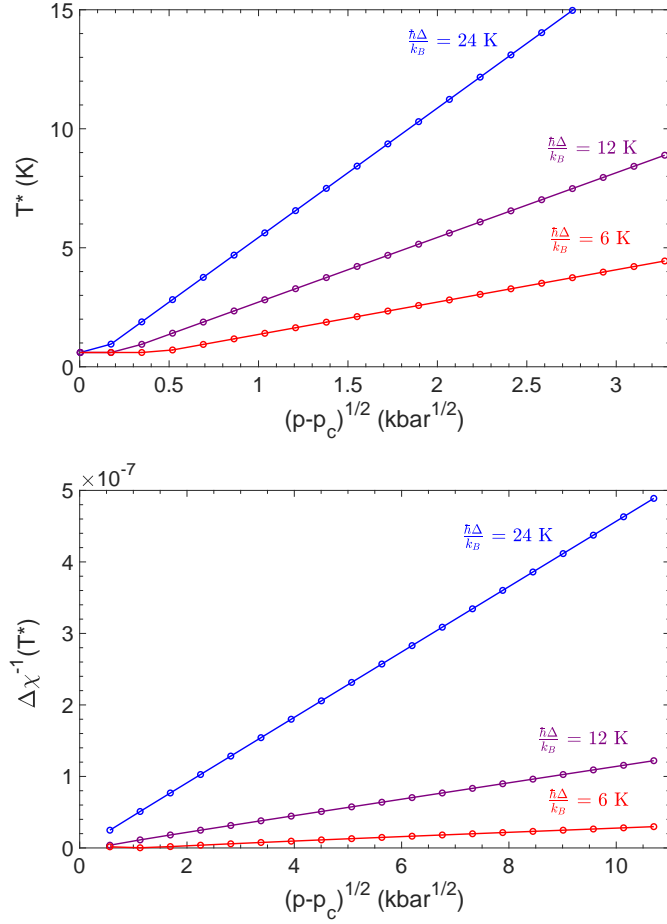
Figure S4: Calculated pressure dependence of the temperature T^* and depth $\Delta\chi^{-1}(T^*)$ of the minimum of the inverse susceptibility vs temperature. Predictions of the self-consistent phonon model including the electrostrictive coupling (Equations 1-4) for T^* vs $(p - p_c)^{1/2}$ (upper) and depth $\Delta\chi^{-1}(T^*)$ vs $(p - p_c)$ (lower) of the inverse susceptibility vs temperature based on the model parameters given in the text, for three values of the zero-pressure gap $\hbar\Delta/k_B = 24$ K (blue), 12 K (purple) and 6 K (red). We see, in particular, that the square of T^* is proportional to the pressure change measured from the ferroelectric quantum critical point at p_c, in agreement with observation (Figure 3a in the main body of the paper). As shown in Figure 2 in the main body of the paper, the inclusion of the contribution of micro-domains can strongly modify the temperature dependence of the inverse susceptibility at low temperatures and significantly modify the depth of the minimum, but has relatively little effect on the position of the minimum and hence on the linear variation of T^* with $(p - p_c)^{1/2}$. The calculations in Figure 2 in the main body of the paper are based on the intermediate value of the three values of the gap quoted above.

180 GPa, so that the dimensionless electrostrictive coupling constant λ defined in Eq S5 is approximately 0.03 (see Ref [28] and references therein). For calculations at finite pressures $\chi^{-1}(0)$ and Δ are replaced, respectively, by $\chi^{-1}(0)(1 - p/p_c)$ and $\Delta(1 - p/p_c)^{1/2}$, while b and v are held constant.

For the calculations including the micro-domain contribution in the electrostrictive coupling model we have assumed a tiny concentration factor c_E of 10 ppb and a scale $\hbar\Delta_E/k_B$ of 0.1 K at ambient pressure. An approximate fit to the data is possible if the ratio c_E/Δ_E^2, which measures the scale of the micro-domain contribution, is assumed to increase approximately linearly with increasing pressure over the experimental pressure range above ambient pressure. In all cases, however, the effective concentration of domains is very tiny and below one part per million.